ORIGINAL PAPER

Microstructure, hardness, and electrical behavior of Y-doped CaZrO$_3$ films prepared by chemical solution deposition

L. A. Dunyushkina · E. O. Smirnova · S. V. Smirnov ·
V. M. Kuimov · S. V. Plaksin

Abstract CaZr$_{0.9}$Y$_{0.1}$O$_{3-\delta}$ films were fabricated by chemical solution deposition on single-crystalline YSZ (ZrO$_2$ doped by 10 mol% of Y$_2$O$_3$) substrates. Mechanical hardness and morphology of the films were studied using nanoindentation and atomic force microscopy techniques. Grain microstructure of the films has been shown to depend upon thermal treatment duration and film thickness. Thin films with grains a few times greater than the film thickness have been obtained. It has been shown that thickness of films can be evaluated by comparing of the indentation curves for the clean and coated by the film substrates. Mechanical hardness of the film has been found to be sensitive to the film grain microstructure. Electrical behavior of CaZr$_{0.9}$Y$_{0.1}$O$_{3-\delta}$ films studied by impedance spectroscopy strongly depends on the film microstructure.

Keywords Y-doped CaZrO$_3$ · Thin films · Film microstructure · Film hardness

Introduction

Acceptor-doped calcium zirconates are known as proton-conducting oxides under hydrogen- and/or water vapor-containing atmosphere at elevated temperatures [1]. They can be used as electrolytes in proton-conducting solid oxide fuel cells or as gas separation membranes if electronic conductivity is significant. Though proton conductivity of CaZrO$_3$-based oxides is less than in cerates of barium and strontium, high mechanical strength and chemical stability even at very low oxygen potentials [2, 3] make zirconates quite attractive materials for application in electrochemical devices. Application of thin films should mitigate relatively high resistance of CaZrO$_3$-based oxides. Additional decrease of resistance is feasible by control of the grain growth process in films since the total resistance of zirconates is mainly determined by the grain boundary resistance [4, 5]. So, fabrication of thin films of proton-conducting oxides with an optimal ratio of thickness and grain size is urgent.

The aim of this research is fabrication of Y-doped CaZrO$_3$ films by chemical solution deposition followed by high-temperature sintering. This technique represents a cost-effective method for synthesizing of high-quality oxide thin films. Single-crystalline YSZ was used as a substrate because CaZrO$_3$ films have good adhesion to YSZ [6]. Besides, use of single-crystalline substrates makes easier study of electrical resistance of the films by the impedance spectroscopy method as there is no effect of the substrate's grain boundaries.

Effect of thermal treatment duration on microstructure, hardness, and electrical properties of the films has been studied. Finding of regularities for the grain growth in CaZrO$_3$-based thin films should promote fabrication of proton-conducting films with large grains and therefore small resistance. A new approach for evaluation of a film thickness has been proposed.

L. A. Dunyushkina (✉) · V. M. Kuimov · S. V. Plaksin
Institute of High Temperature Electrochemistry,
Russian Academy of Sciences Urals Branch,
20, Academicheskaya St.,
620990 Ekaterinburg, Russia
e-mail: lidung@list.ru

E. O. Smirnova · S. V. Smirnov
Institute of Engineering Science,
Russian Academy of Sciences Urals Branch,
34, Komsomolskaya St.,
620990 Ekaterinburg, Russia

Experimental

Films of CaZr$_{0.9}$Y$_{0.1}$O$_{3-\delta}$ were prepared by chemical solution deposition on single-crystalline YSZ substrates. The coating solution was prepared by dissolution of Ca

$(NO_3)_2 \times nH_2O$, $ZrOCl_2 \times 8H_2O$, and $Y_2(NO_3)_3 \times nH_2O$ (all with 99.99 % purity) in ethanol. A single crystal of YSZ with a cubic structure (a=5.135Å) sintered in Physical Institute of Russian Academy of Science (Russia) was cut in a parallel way in square plates of $5 \times 5 \times 0.5$ mm^3. These plates were used as substrates. The angular deviation between the surface of the plates and (311) crystallographic planes was close to 10°. The substrates were polished and annealed at 1,100 °C to remove surface contamination. After that the substrates were dipped in the dip-coating container and then removed from the solution at a withdrawal rate of 2 mm/min. After drying for 5 min, the films were calcined at 800 °C for 1 h. To get the films with various thicknesses, the "deposition–calcining" procedure was repeated for two and eight times. Subsequently, the specimens were exposed to a final annealing at 1,000 °C for various durations, from 2 to 30 h, to get various grain sizes in the films. Phase composition of the sintered films was checked by X-ray diffraction in sliding beams with an angle of incidence of 1.5° (D-Max 2200, Rigaku, Japan, $CuK_{\alpha 1}$).

Mechanical hardness, surface roughness, and morphology of the films were studied using TI 900 Triboindenter (Hysitron, USA) equipped with an atomic force microscopy (AFM) imaging option. Nano-indentation tests were carried out using the load control mode with the indentation load in the range of 500–10,000 μN. For each test, it took 15 s for the loading process. For each load value, five or more indentations have been performed.

A hardness number H is calculated as

$$H = P/A, \tag{1}$$

where P is the maximum applied load and A is a contact area between the sample and the indenter. For an ideal pyramidal geometry tip, A is determined as

$$A = 24.5 \times h^2, \tag{2}$$

where h is the maximum indentation depth reached by the indenter during the indentation test.

For thin films, true determination of mechanical strength is rather complicated. A general rule is that applied mechanical loads are to be so small that not to exceed 10–20 % of a film thickness in indentation experiments to avoid plastic deformation of a substrate. However, as was shown in [7] for soft films on hard substrates, an indentation depth can be significantly greater, e.g., for aluminum film on silicon, a relative indentation depth of more than 30 % of a film thickness gave negligible deviations from the true film hardness. At the same time, the film's surface roughness is to be small as the roughness leads to scatter of hardness values. An indentation depth has to be about 20 times of an average roughness of film's surface in order

to keep the uncertainty in the contact area between the indenter and the film within 5 % [8]. These requirements make limitations for thickness and surface roughness of the film. Roughness parameters were calculated from the topographic profiles obtained by scanning probe microscopy included in TI 900. Roughness was measured in selected areas of 100 μm^2. The thickness of the films was evaluated by comparing of the indentation curves obtained for clean and covered by the film substrates.

The effect of the film microstructure on the across-film electrical behavior of $CaZr_{0.9}Y_{0.1}O_{3-\delta}$ films was studied by the two-probe a.c. impedance method in a frequency range 1 MHz–0.1 Hz using Parstat 2273-SVS analyzer (Advanced Measurement Technology Inc., USA). For these measurements, the symmetric cells Ag/film/YSZ/film/Ag with films annealed for 2, 10 and 30 h were prepared by painting of Ag paste on both sides the film/YSZ/film specimens with the following annealing at 700 °C. For comparison, the symmetric cell Ag/YSZ/Ag was prepared.

Results and discussion

Phase composition of the film

X-ray diffraction study has shown that $CaZr_{0.9}Y_{0.1}O_{3-\delta}$ film deposited on a single-crystalline YSZ and sintered at 800 °C for 1 h is single phase with a $CaZrO_3$ perovskite structure. No reflections from the single-crystalline YSZ substrate were observed in the investigated 2θ interval (Fig. 1).

Film thickness

Figure 2 schematically shows loading curves for a hard substrate and a relatively soft film. A solid line representing a loading curve for the film/substrate sample is to be determined by the film at small load values, while at high loads, when an indentation depth more than the film thickness, the
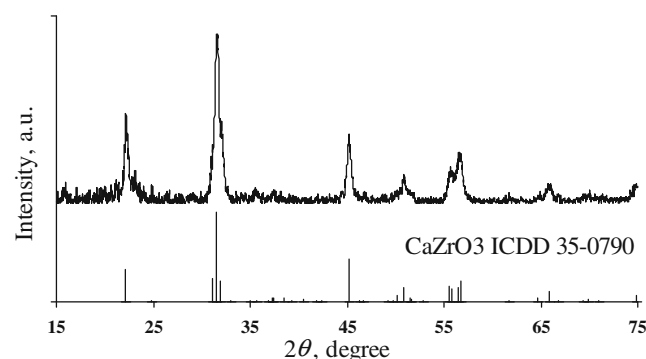
Fig. 1 X-ray diffraction pattern of $CaZr_{0.9}Y_{0.1}O_{3-\delta}$ film deposited on single-crystalline YSZ
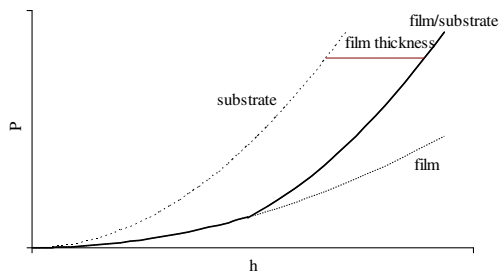
Fig. 2 Schematic loading curves for a hard substrate, a soft film, and for the film deposited on the substrate

shape of the curve is to be determined by the substrate. As can be seen in Fig. 2, at high loads, the loading curve for the film/substrate repeats the shape of the curve for the clean substrate with a shift along h-axis equaled to the film thickness. So, the film thickness can be evaluated from the shift between the loading curves for the clean substrate and for the coated by a film substrate under high loads.

Figure 3 shows the indentation curves for the single-crystalline YSZ substrate and for $CaZr_{0.9}Y_{0.1}O_{3-\delta}$ films deposited on the single-crystalline YSZ for two and eight times. Both films were annealed at 1,000 °C for 30 h. For the thicker film, data for several maximal loads are given. The film thickness values, estimated from these data, are 45 ± 5 and 150 ± 10 nm.

The load–depth curves in logarithmic scale (Fig. 4) show that for YSZ, $\ln P$ rises linearly with $\ln h$ as predicted by Eqs. 1 and 2. Some deviation from linearity at small loads/depths (at $\ln h < 3$, or $h < \sim 20$ nm) can be caused by a number of reasons, e.g. a round tip of a "nominally" sharp Berkovich indenter [9], a surface roughness, or presence of a surface layer with different structure and properties. For the film/YSZ samples, $\ln P$–$\ln h$ dependencies are linear at high load/depth values, but at some value of the indentation depth significant deviation from linearity is observed, which is obviously caused by the film coating. The inflection
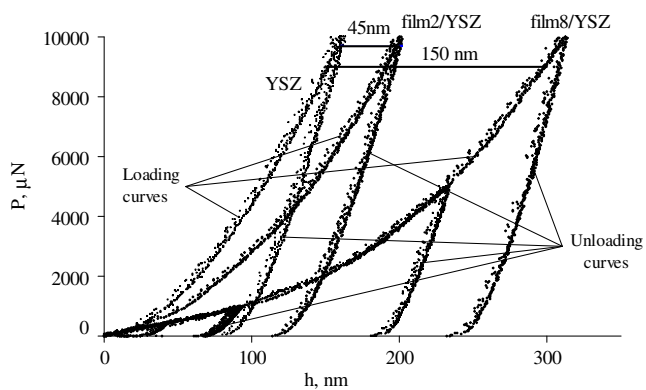
Fig. 3 Loading–unloading curves for the single-crystalline YSZ and for $CaZr_{0.9}Y_{0.1}O_{3-\delta}$ films deposited on the single-crystalline YSZ for two and eight times. For the thick film, the data for several maximal loads are shown
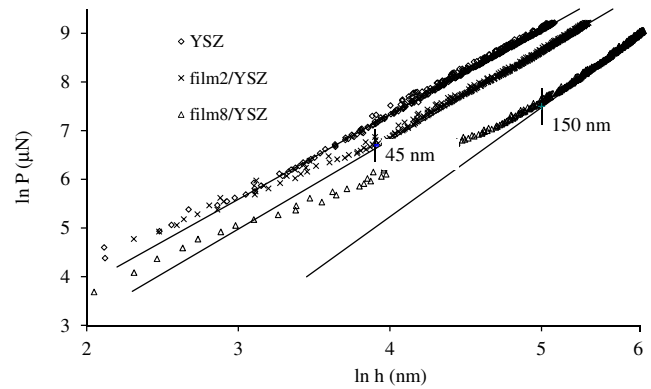
Fig. 4 Loading curves in logarithmic scale for the single-crystalline YSZ and for $CaZr_{0.9}Y_{0.1}O_{3-\delta}$ films deposited on the single-crystalline YSZ for two and eight times
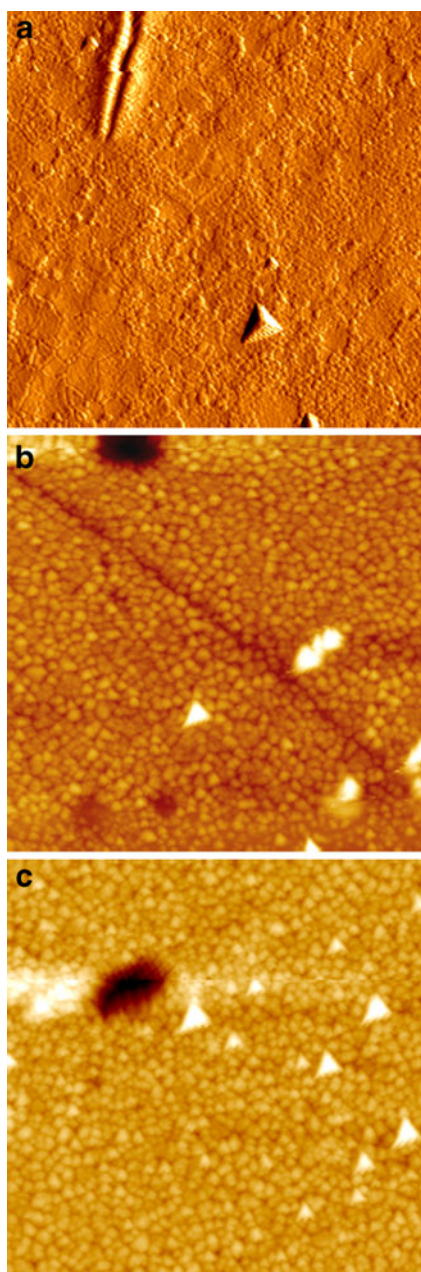
points correspond to about 45 and 150 nm for the thin and thick films, respectively, which well agree with the values of the film thickness obtained above.

Grain microstructure of films

Top view AFM images of $CaZr_{0.9}Y_{0.1}O_{3-\delta}$ films annealed at 1,000 °C for various durations (Fig. 5) display granular microstructure of the films. As was mentioned above, the films were exposed to prolonged thermal treatment at 1,000 °C, from 10 to 30 h, to get large grains. The AFM picture of the film with thickness of 150 nm annealed for 30 h (Fig. 5a) shows a network of grains of about 150 nm together with very large grains up to 700–800 nm which exceeds a few times the film thickness.

Usually, in thin films, three-dimensional normal grain growth occurs till average grain size is small comparing to the film thickness; once the average grain size becomes comparable with the film thickness, the rate of the grain growth slows and stops resulting in a stagnant grain structure in which all grain boundaries intersect both the top and bottom surfaces of the film [10, 11]. Subsequent process of grain growth, if it is observed, is called abnormal grain growth. In case of abnormal grain growth, a small fraction of grains continues to grow at the expense of neighboring normal grains [10]. The grain pattern of the film presented in Fig. 5a shows that during thermal treatment first grained microstructure with the grain size close to the film thickness develops, and then the process of abnormal grain growth occurs resulting in the large-grain structure of the film.
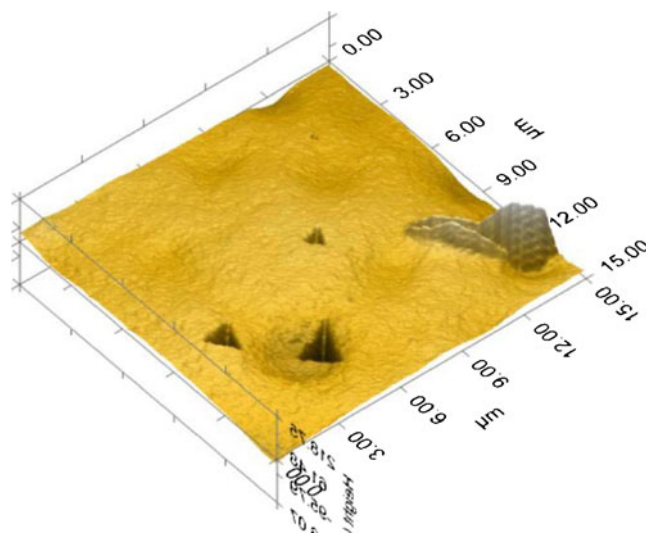
The films with thickness of 45 nm treated for 10 and 30 h show similar grain size distributions: the lateral size varies from 200 to 400 nm with a major number of grains of about 300 nm (Fig. 5b, c). Thus, the lateral size of grains exceeds a few times the film thickness as

Fig. 6 AFM image of 45 nm $CaZr_{0.9}Y_{0.1}O_{3-\delta}$ film after indentation

thickness, so for energy loss decrease in the film-based electrochemical devices, it is reasonable to reduce the film thickness. However, in thicker films, the grain boundary resistance can be less due to greater grains. As far as at moderate temperatures the grain boundary resistance usually mitigates the total resistance in oxides, it is needful to search an optimal thickness/grain size ratio for each film's composition.

Film hardness

As was discussed in the "Experimental" section, for true determination of film's hardness, a surface roughness of the film should be at least 20 times less than an indentation depth. An average surface roughness of

Fig. 5 AFM images 10×10 μm^2 of the $CaZr_{0.9}Y_{0.1}O_{3-\delta}$ films after thermal treatment at 1,000 °C: **a** 150 nm film annealed for 30 h; **b** 45 nm film annealed for 10 h; **c** 45 nm film annealed for 30 h

for the former film, which also can be explained by the abnormal grain growth. However, it seems that in 45 nm film, the process of abnormal grain growth is completed after 10-h thermal treatment, while in 150 nm film, the process is not completed after 30 h. Evidently that in the thinner film, the abnormal growth of grains completes faster.

Summarizing these data we can draw a conclusion that calcium zirconate films with grains significantly greater than the film thickness can be prepared by long thermal treatment. As electrical resistance of a film is proportional to the film
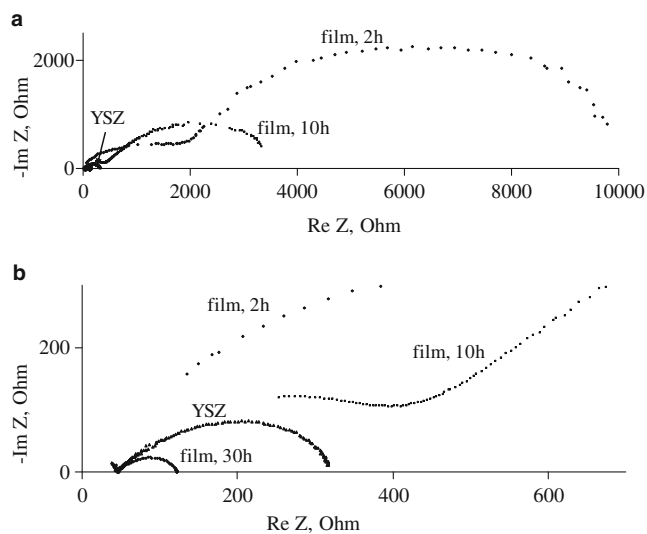
Fig. 7 Impedance spectra for Ag/film/YSZ/film/Ag symmetric cells with the $CaZr_{0.9}Y_{0.1}O_{3-\delta}$ films annealed at 1,000 °C for 2, 10 and 30 h, and for Ag/YSZ/Ag cell with the single-crystalline YSZ, at 600 °C: (**a**) total spectra; (**b**) a fragment with a higher magnification

$CaZr_{0.9}Y_{0.1}O_{3-\delta}$ films varied from 1.9 to 6.0 nm depending mostly on presence of pores or scratches on the substrate as well as a number of the film layers; the film surface roughness decreases with a number of film deposition cycles. For hardness determination, the most flat films with a roughness of about 2 nm were selected to minimize an error. In this case, a reliable value of the film's hardness can be obtained at the indentation depth of at least 40 nm.

Another limitation for the film hardness determination is related with a film thickness. The minimal indentation depth of 40 nm is about 25 % of 150 nm film which gives an increasing hardness error. However we have to note that a real hardness of the film might be somewhat higher as elastic deformation of the substrate under high indentation depth contributes to the indent area which makes the calculated value of hardness less (see Eq. 1).

A hardness value determined for 150 nm $CaZr_{0.9}Y_{0.1}O_{3-\delta}$ film annealed for 30 h at the indentation depth of 40 nm is equal to 7.5±0.5 GPa. The film of the same thickness but annealed for 10 h at the same temperature has shown a hardness of 6.0±0.4 GPa. The obtained hardness values of $CaZr_{0.9}Y_{0.1}O_{3-\delta}$ films are significantly higher than Vickers hardness of the small-grained $CaZrO_3$ film obtained by chemical solution deposition on polycrystalline YSZ and thermal treatment at 1,000 °C for 1 h, 3.8 GPa [6]. Considerable discrepancy in hardness values of $CaZrO_3$-based films is obviously conditioned by different grain morphology of the films. The films with greater grains possess higher hardness. A hardness value for the single-crystalline YSZ determined from the data shown in Fig. 3 at a maximal load of 0.01 N is 22.3±0.6 GPa.

AFM image of $CaZr_{0.9}Y_{0.1}O_{3-\delta}$ film after indentation show plain and homogeneous coating, however some cracks can be observed (Fig. 6). Though the indenter penetrated into the substrate during most indentation tests, no brittle fracture, cracking, or delaminating near indentation stamps were observed, which testifies to good adhesion of the film.

Across-film electrical behavior of $CaZr_{0.9}Y_{0.1}O_{3-\delta}$ films

The complex impedance spectra for the cells Ag/film/YSZ/film/Ag with 150 nm films annealed for 2, 10, and 30 h measured at 600 °C are shown in Fig. 7. For comparison, the data for the Ag/YSZ/Ag cell are given. For the latter cell, the high-frequency process corresponds to the YSZ bulk resistance and the low-frequency semicircle is related with the electrode polarization. As can be seen in Fig. 7, the electrochemical performance of the cells with films strongly depends on the thermal treatment duration of the films and, therefore, on their grain microstructure: the total resistance of the cell Ag/film/YSZ/film/Ag with the film annealed for 30 h is 2.5 times less than for the cell Ag/YSZ/Ag (Fig. 7b), while thermal treatment of the film for 2 h leads to increase of the cell total resistance for a few orders (Fig. 7a). Detailed interpretation of the impedance data for the films is rather complicated due to presence of various charge carriers (protons, oxygen ions and holes) in $CaZr_{0.9}Y_{0.1}O_{3-\delta}$; this is a subject of our next paper.

Conclusions

$CaZr_{0.9}Y_{0.1}O_{3-\delta}$ films were fabricated by chemical solution deposition. It has been shown that grain microstructure and mechanical hardness of the films can be improved by long thermal treatment. Thin films with grains significantly greater than the film thickness have been obtained. Hardness values of $CaZrO_3$-based films have been shown to depend on the grain morphology of the films; the film with greater grains has higher hardness. A new approach for evaluation of a film thickness based on analysis of the load–indentation depth curves for the clean and covered by the film substrates has been proposed.

The coarse-grained microstructure of proton-conducting oxide films gives an appreciable advantage in the film electrical behavior. In the next paper, we will report the extensive results of the electrical properties study for proton-conducting oxide films.

References

1. Yajima T, Kazeoka H, Yogo T, Iwahara H (1991) Solid State Ionics 47:271–275
2. Iwahara H (1995) Solid State Ionics 77:289–298
3. Yajima T, Suzuki H, Yogo T, Iwahara H (1992) Solid State Ionics 51:101–107
4. Hwang SC, Choi GM (2006) Solid State Ionics 177:3099–3103
5. Mukundan R, Brosha EL, Birdsell SA, Costello AL, Garzon FH, Willms RS (1999) J Electrochem Soc 146:2184–2187
6. Dunyushkina L, Plaksin S, Pankratov A, Kuzmina L, Kuimov V, Gorelov V (2011) Russ J Electrochem 47:1274–1280
7. Cai X, Bangert H (1995) Thin Solid Films 264:59–71
8. Fischer-Cripps AC (2002) Nanoindentation. Springer, Berlin
9. Suresh S, Nieh T-G, Choi BW (1999) Scr Mater 41:951–957
10. Thompson CV (1990) Annu Rev Mater Sci 20:245–268
11. Heiroth S, Frison R, Rupp JLM, Lippert T, Meier EJB, Gubler EM, Döbeli M, Conder K, Wokaun A, Gauckler LJ (2011) Solid State Ionics 191:12–23